

Micro-damage instability mechanisms in composite materials: Cracking coalescence versus fibre ductility and slippage

International Journal of Damage

Mechanics

0(0) 1–21

© The Author(s) 2024

Article reuse guidelines:

sagepub.com/journals-permissions

DOI: 10.1177/10567895241297313

journals.sagepub.com/home/ijd**Alberto Carpinteri and Federico Accornero** 

Abstract

The load-displacement softening response of quasi-brittle solids exhibits an unstable structural behavior, which is characterised by a negative slope in the post-peak regime. In severely brittle situations, the post-peak behaviour can show a virtual positive slope, the fracture propagation occurring unexpectedly with a catastrophic loss in the load-carrying capacity. In this case, if the displacement controls the loading process, the curve exhibits a discontinuity and the representative point drops to the lower branch with a negative slope. On the other hand, in order to obtain a stable crack growth, a decrease both in load and in displacement is required. In the last forty years, in-depth study of the so-called snap-back instability was conducted in relation to crack propagation phenomena in quasi-brittle materials. In the present work, the structural response of two brittle-matrix specimens is analysed: the first contains a distribution of collinear micro-cracks, whereas the second presents multiple parallel reinforcing fibres embedded in the matrix. In both cases, it is shown that the structural response presents a discrete number of snap-back instabilities with related peaks and valleys, the crack propagation occurring alternately within the matrix and through the heterogeneities. Thus, the strong analogy between weakened and strengthened zones consists in a multiple snap-back mechanical response, where descending branches of propagating cracks alternate with ascending (linear) branches of arrested cracks.

Keywords

Brittleness, coalescence, fibre-reinforced materials, scale effects, snap-back

Introduction

The load-displacement softening response of quasi-brittle solids exhibits an unstable structural behaviour, which is characterised by a negative slope in the post-peak regime. In severely brittle situations, the post-peak behaviour can show a virtual positive slope, the fracture propagation

Department of Civil Engineering and Intelligent Construction, Shantou University, Shantou, China

Corresponding author:

Federico Accornero, Shantou University, 243 University Road, Shantou 515063, China.

Email: federico@stu.edu.cn

occurring unexpectedly with a catastrophic loss in the load-carrying capacity. In this case, if the displacement controls the loading process, the curve exhibits a discontinuity and the representative point drops to the lower branch with a negative slope. On the other hand, in order to obtain a stable crack growth, a decrease both in load and in displacement is required. In the last forty years, in-depth study of the so-called snap-back instability was conducted in relation to crack propagation phenomena in quasi-brittle materials (Carpinteri, 1984, 1989a, 1989b, 2021). In the framework of the Cohesive Crack Model, the cusp catastrophe represents the classical Griffith and Irwin instability according to Linear Elastic Fracture Mechanics (LEFM) for very brittle conditions.

To introduce a multiple snap-back mechanical response, consider a tension test specimen containing a distribution of collinear micro-cracks, as illustrated in Figure 1(a). In addition, consider the case of a specimen where parallel reinforcing fibres are embedded in the matrix, as illustrated in Figure 1(b). A load P is applied that opens the faces of an edge crack that propagates through the collinear micro-cracks or through the parallel fibres. The propagation occurs alternately through the matrix and the heterogeneities (Carpinteri and Accornero, 2018, 2019), the process being controlled by a monotonically increasing crack growth.

In both cases, the structural response is characterized by a discrete number of snap-back instabilities, showing peaks and valleys (Figure 1(c)). After each single peak, the crack starts growing in the matrix. Thus, the descending branches after the peaks describe the crack growth between a micro-crack tip and the next, or between a fibre and the next. The crack arrests at the minimum of each valley, which represents the achievement of the next crack tip or fibre (Figure 1(a) and (b)). The analogy between weakened and strengthened zones consists therefore in a multiple snap-back mechanical response, where descending branches of propagating cracks alternate with ascending (linear) branches of arrested cracks.

Cohesive crack model and snap-back instability

The traditional definition of strength —intended as force per unit area that causes failure— needs to be revised in light of the latest cutting-edge scientific developments in the field of materials mechanics, which arose for the first time in the second half of the 20th Century. This is especially true when

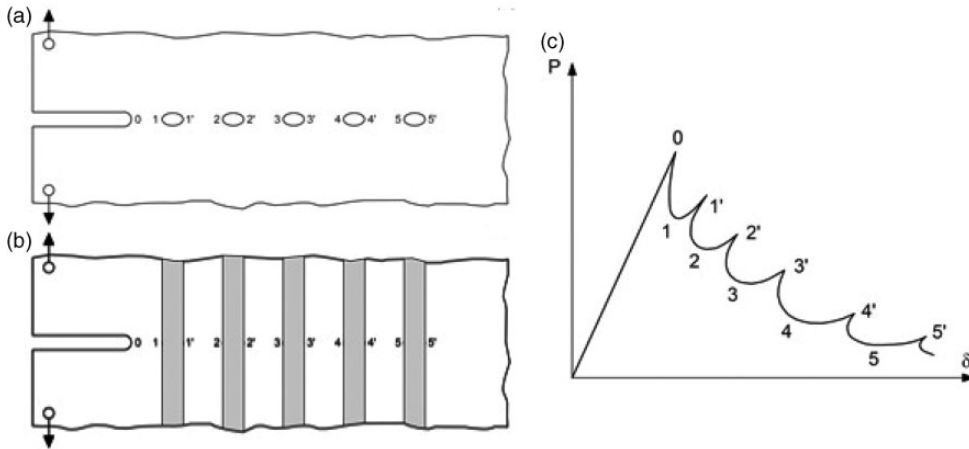


Figure 1. Brittle specimen with an edge crack and collinear micro-cracks (a); Regular distribution of parallel reinforcing fibres in a brittle-matrix specimen with an edge crack (b) and Load-displacement response diagram (c).

dealing with structures that are particularly large or small. To effectively determine the ductility or the brittleness of a structure, the strength of the material must be compared to other properties, such as the toughness in the event of fracturing processes, together with the structural size (Carpinteri, 1981, 1982, 1984, 1984, 1989, 1989, 2021). It is important to distinguish between the simple thickness effect, which takes into account the variations in fracture toughness with the specimen thickness, whilst maintaining constant the remaining planar sizes, and the scale effect as the competition between two distinct collapses governed by generalized forces with different physical dimensions. The first descends from a transition between plane stress and plane strain conditions (Carpinteri and Accornero, 2021). Both these effects are interacting in metals, whereas only the scale effect is present in concrete-like materials (Bigaj and Walraven, 1993; Goldstein and Vainshelbaum, 1978; Kani, 1967; Tanabe et al., 2004; Tang et al., 1992).

The minimal basis for predicting the structural response consists of taking into account two intrinsic properties of the material plus a geometrical characteristic of the structure. In strict analogy to the change from plastic collapse to buckling instability in structures subjected to compression as their slenderness increases, so there is a transition from plastic collapse to brittle fracture in structures subjected to tension as size-scale increases.

Glass filaments and Liberty ships are two prominent examples of the abovementioned properties. Liberty ships, which were largely exploited during the Second World War, split into two parts without warning (Figure 2(a)). The contrast between the significant brittleness involved in these failures and the high ductility displayed by specimens of the same steel in the laboratory caused profound astonishment in technicians and researchers at the time (Gordon, 1975; Tassava, 2003; Thomason and Vlug, 1996; Tipper, 1962). Conversely, it has been demonstrated that a microscopic filaments of glass used for fibre-reinforcement can withstand large strains and stresses up to two orders of magnitude greater than the tensile strength of the glass itself (Figure 2(b)). These two examples highlight the striking relationship between strength, ductility, and the structural size-scale: brittleness and low strength can define large steel structures, whereas ductility and high strength characterise microscopic glass structures. On the other hand, it is commonly recognized that glass is a particularly brittle material, whereas steel is a relatively ductile material when tested in laboratory.

Furthermore, a ductile-to-brittle transition occurring when the specimen size increases has been observed, even at the laboratory scale. Increasing the size-scale entails a clear transition towards brittle structural behaviour, which is actually observed for all materials, whether they are metal, polymer, ceramic, or cement (Carpinteri, 2021). This transition is accompanied by a sudden drop in

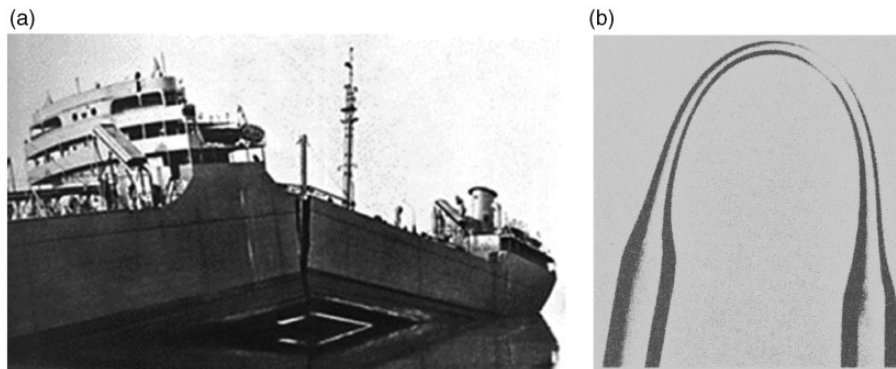


Figure 2. Brittle failure of a large-scale steel hull (a) and Ductile behaviour of small-scale glass fibre (b).

the loading capacity and a rapid crack propagation if the material and the geometrical shape remain unchanged. However, it is worth noting that specimens with relatively small dimensions exhibit ductile behaviour and slow crack development (Figure 3).

As anticipated, very complex phenomena can affect the load vs. displacement relationship of a structure: snap-through instability, defined as a loss of stability in the controlled load condition, and snap-back instability, representing a loss of stability in the controlled displacement condition. Such phenomena are very general, and usually encountered in structural problems characterized by either geometrical or mechanical non-linearities. As an example, they may appear in the buckling response of elastic structures, as evidenced in the work by von Kármán and Tsien (von Kármán and Tsien, 1941) for thin cylindrical shells under axial compression (Figure 4).

On the other hand, snap-back instabilities can be encountered when materials exhibiting strain-softening behaviours are considered (Rots and de Borst, 1987). This is, for instance, the case of plain

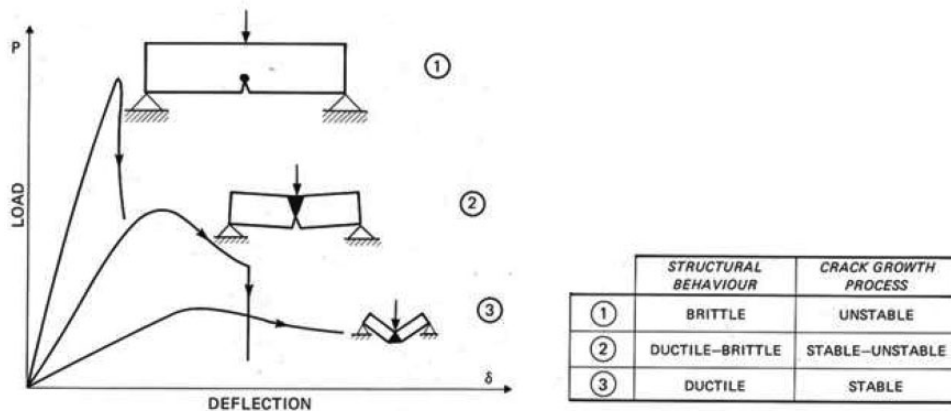


Figure 3. Ductile-to-brittle transition by increasing the specimen size.

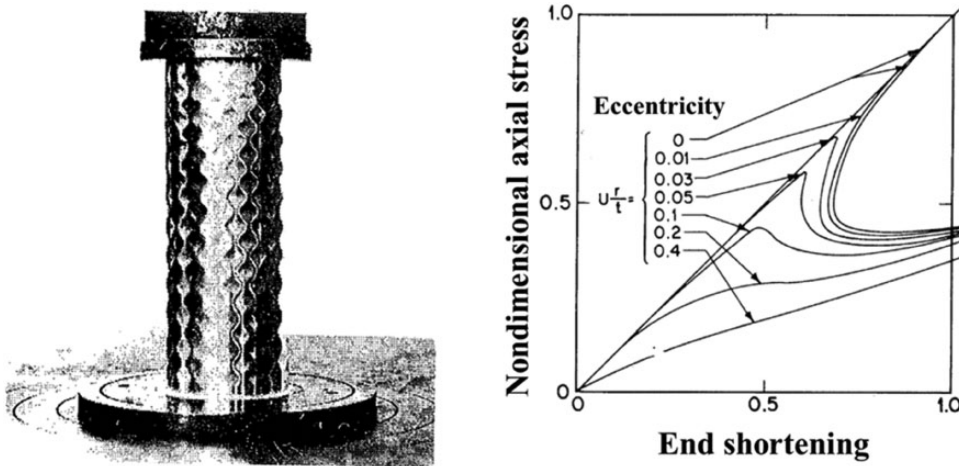


Figure 4. Buckling of thin cylindrical shells under axial compression (von Kármán and Tsien, 1941).

concrete slabs in tension (Figure 5(a)), whose overall responses are highly influenced by the softening behaviour of the process zone (Figure 5(b)), the latter being governed by the fracture energy of the material, G_F .

In the following, we consider an elastic-softening tie made by a material with a double constitutive law: being E the elastic modulus, the constitutive law is described as tension σ versus dilation ε , and, after attainment of ultimate tensile strength σ_u or strain $\varepsilon_u = \sigma_u/E$, we have tension σ versus crack opening displacement w (Figure 5(b)).

If a plane slab of elastic-softening material is increasingly loaded, three deformation histories will arise after the ultimate tensile strength σ_u is reached, depending on its characteristic structural size l (Figure 6): (1) normal softening, when $w_c > \varepsilon_u l$; (2) vertical drop, when $w_c = \varepsilon_u l$; (3) snap-back, when $w_c < \varepsilon_u l$.

Briefly, the global brittleness of the slab can be defined as the ratio of ultimate elastic energy at the peak load contained in the body to the energy dissipated by fracture:

$$\text{Brittleness} = \frac{\sigma_u^2}{2E} \times \text{Area} \times l / (G_F \times \text{Area}) \propto \frac{\sigma_u^2 l}{EG_F} \quad (1)$$

This dimensionless quantity is higher than the unity when $w_c < \varepsilon_u l$ (specimen n. 3 in Figure 6) and a catastrophic softening instability occurs.

In this context, the analytical and numerical investigations carried out by the first author in (Carpinteri, 1989) put into evidence a transition from softening to snap-back instability either by increasing the specimen dimensions and/or the material strength, and/or by decreasing the material fracture energy, i.e., when $\frac{G_F}{\sigma_u l} = s_E \rightarrow 0$, being s_E the so-called Energy Brittleness Number introduced in the framework of the Cohesive Crack Model. Thus, it is worth noting that equation (1) becomes: $\text{Brittleness} = \frac{\sigma_u^2 l}{EG_F} = \frac{\varepsilon_u}{s_E}$.

The post-peak catastrophic branch shown in Figure 6, which is a bifurcation of the global equilibrium characterized by a positive slope in the load vs. displacement diagram, can be captured only if the loading process is controlled by an increasing function of time.

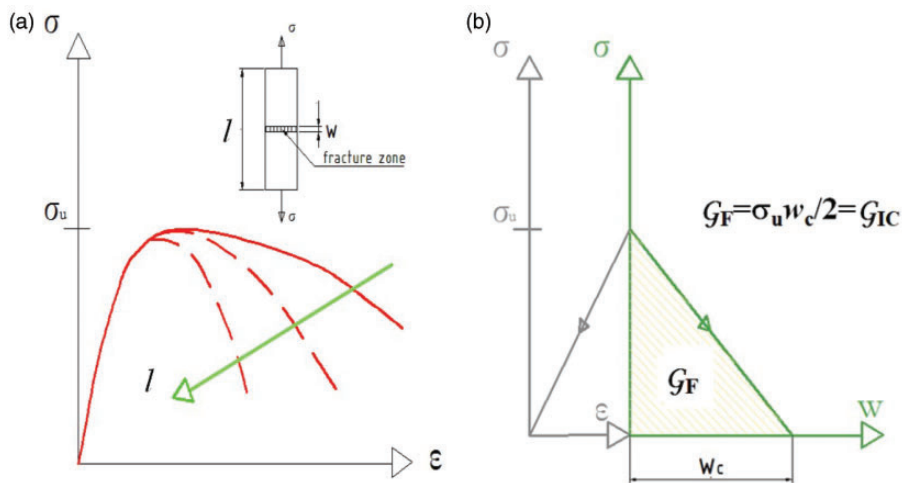


Figure 5. Softening due to damage localization: Ductile-to-brittle transition influenced by the length of the specimen (a) and Stress-strain vs cohesive behaviour (b).

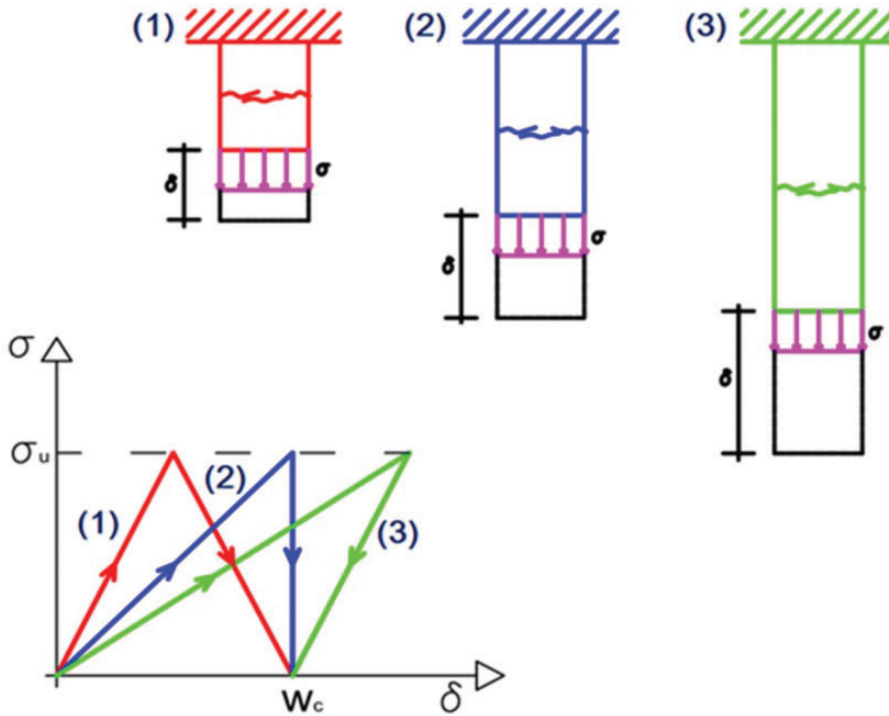


Figure 6. Plane slab in tension: Normal softening (1), vertical drop (2), and snap-back (3).

Moreover, it is interesting to remark how this cusp catastrophe, as described by the Cohesive Crack Model, can represent the classical Griffith and Irwin instability (LEFM) for very brittle conditions. In general, all the geometrical features of the specimen influence the global ductility (or brittleness), and particularly slenderness and size-scale. In Figure 7, a three-point bending scheme of an initially cracked (a) and initially uncracked (b) beam with depth b and length ℓ is reported. For the notched beam, the critical situation in very brittle cases (LEFM) is triggered when the stress-intensity factor attains the material fracture toughness, $K_I = K_{IC}$, whereas, for the initially uncracked beam, the critical situation is set by $\sigma_{\max} = \sigma_u$. The structural behaviour of both the specimens depicted in Figure 7 can be analysed by means of the Cohesive Crack Model.

In particular, a negative slope of the post-peak load-displacement curve (normal softening) will occur for relatively large values of s_E (Figure 8(a)), whereas a positive slope of the post-peak load-displacement curve (snap-back) is related to $s_E = \frac{G_F}{\sigma_u b} \rightarrow 0$. It can be demonstrated that, for low s_E values, the results of the Cohesive Crack Model tend to those of LEFM with regard to the cuspidal point in Figure 8(b): in this case, if the loading process is controlled by the deflection, the P versus δ curve will show a discontinuity in its bearing capacity with global instability.

In addition, it is worth noting that, by keeping s_E unchanged, a post-peak softening behaviour (Figure 8(a)) can characterise the case of large initial crack depth, a_0/b , or low specimen slenderness, ℓ/b , whereas a bifurcation of the global equilibrium (Figure 8(b)) arises for small initial crack depth, a_0/b , or high beam slenderness, ℓ/b .

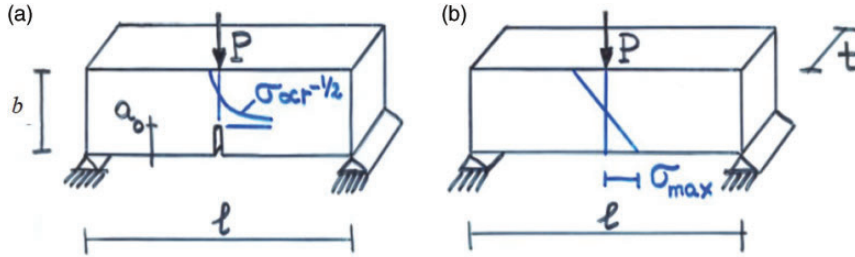


Figure 7. (a) Stress-singularity in an initially cracked specimen and (b) Navier stress distribution in an initially uncracked specimen.

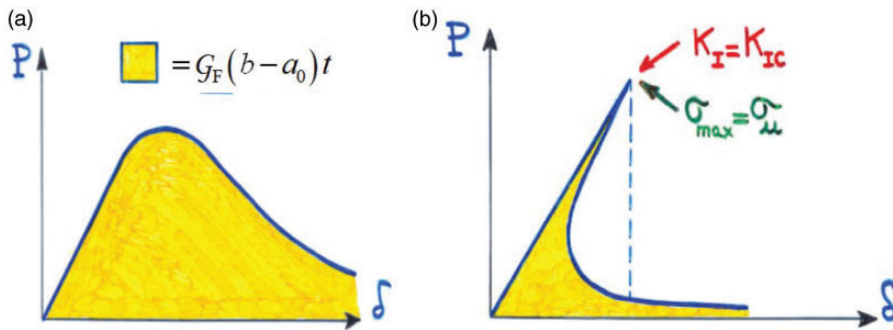


Figure 8. The crucial role of the brittleness number: (a) Normal softening ($s_E = \frac{G_F}{\sigma_u b} \rightarrow \infty$) and (b) Snap-back ($s_E = \frac{G_F}{\sigma_u b} \rightarrow 0$).

Virtual crack propagation in brittle materials

Due to different physical dimensions of ultimate tensile strength, σ_u , and fracture toughness, K_{IC} , scale effects are always present in the usual fracture testing of common engineering materials. This means that, for the usual scale of the laboratory specimens, the ultimate strength collapse or the plastic collapse at the ligament tends to anticipate and obscure the brittle crack propagation. Such a competition between collapses of a different nature can easily be shown by considering the ASTM fracture toughness evaluation formula for the three-point bending test (Carpinteri, 1982):

$$K_I = \frac{P\ell}{tb^{3/2}} f\left(\frac{a}{b}\right) \quad (2)$$

where b is the beam depth, t the beam thickness, and ℓ the beam span, whereas P is the external force, and $f\left(\frac{a}{b}\right)$ represents a suitable shape function.

At the moment of potential collapse due to brittle crack propagation, equation (2) becomes

$$K_{IC} = \frac{P_{max}\ell}{tb^{3/2}} f\left(\frac{a}{b}\right) \quad (3)$$

where P_{max} is the external load of brittle fracture.

If both members of equation (3) are divided by $\sigma_u b^{1/2}$, we obtain (Carpinteri, 1980; Carpinteri, 1982; Carpinteri and Accornero, 2021)

$$\frac{K_{IC}}{\sigma_u b^{1/2}} = \frac{P_{\max} \ell}{\sigma_u t b^2} f\left(\frac{a}{b}\right) \quad (4)$$

Denoting by

$$s = \frac{K_{IC}}{\sigma_u b^{1/2}} = \left(\frac{s_E}{\varepsilon_u}\right)^{1/2} \quad (5)$$

the so-called Brittleness Number (Carpinteri, 1982), we have:

$$\frac{P_{\max} \ell}{\sigma_u t b^2} = \frac{s}{f\left(\frac{a}{b}\right)} \quad (6)$$

On the other hand, we can consider the force P that potentially produces ultimate strength collapse in the ligament as:

$$\frac{1}{4} P_{\max} \ell = \sigma_u t \frac{(b-a)^2}{6} \quad (7)$$

from which follows, in nondimensional form

$$\frac{P_{\max} \ell}{\sigma_u t b^2} = \frac{2}{3} \left(1 - \frac{a}{b}\right)^2 \quad (8)$$

The diagrams of equations (6) and (8) are presented in Figure 9 as functions of the initial relative crack depth a/b .

Whilst the former of these equations gives a family of curves as the nondimensional number s varies, the latter is represented by a single curve (thick line). When $s < 0.50$, it may be noted how the ultimate strength collapse precedes the brittle crack propagation both for sufficiently short cracks or sufficiently long ones. Whilst the first tendency is typical of LEFM, the second represents a new, non-intuitive development. It is basically due to the unlikelihood of a singular stress distribution developing in the cases where there is an excessively reduced ligament. As the number s increases, the interval of a/b for which brittle propagation of the crack precedes ultimate strength collapse shrinks until it vanishes for $s = 0.50$, the value for which the corresponding fracture curve is tangent to the curve of ultimate strength collapse. For $s > 0.50$, ultimate strength collapse precedes brittle crack propagation for any relative crack length, there existing no points of intersection between the fracture curve and the ultimate strength collapse curve. This means that a true LEFM collapse occurs only for comparatively low fracture toughnesses, high tensile strengths, and/or large structure sizes. If the material ductility can always be calculated using the ratio K_{IC}/σ_u (Barenblatt, 1962), the size-scale must also be included into the formulation in order to determine the ductility of the structure. The most synthetic way of characterizing the degree of ductility in a structure is the Brittleness Number s given by equation (5). Therefore, plastic limit analysis turns out to be a

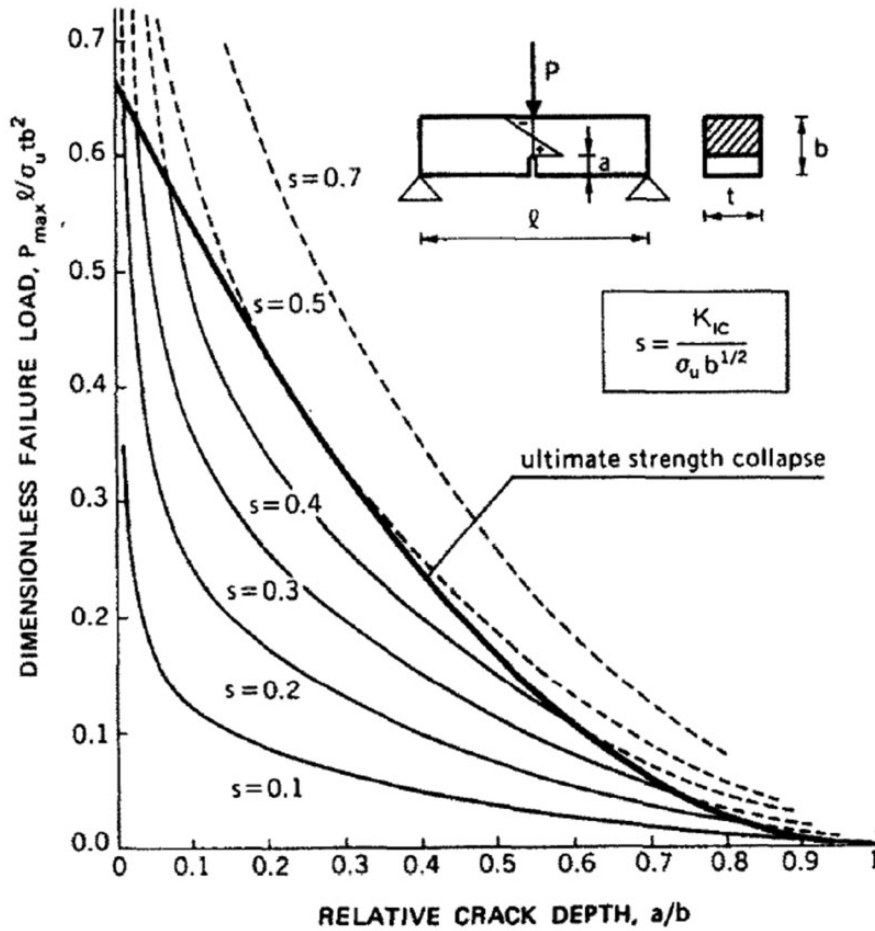


Figure 9. Nondimensional load of crack instability versus initial relative crack depth.

valid method of assessment only when the structure under examination has a Brittleness Number that is not excessively low.

The flexural behaviour of the beam depicted in Figure 9 will be analyzed in the following. The deflection due to the elastic compliance of the uncracked beam is

$$\delta_e = \frac{P\ell^3}{48EI} \quad (9)$$

where E is the material Young's modulus, and I is the moment of inertia of the beam cross-section. On the other hand, the deflection due to the local crack compliance is (Tada et al., 1973):

$$\delta_c = \frac{3}{2} \frac{P\ell^2}{tb^2E} g\left(\frac{a}{b}\right) \quad (10)$$

where $g\left(\frac{a}{b}\right)$ represents a suitable shape function.

The Superposition Principle provides $\delta = \delta_e + \delta_c$, and, in nondimensional form

$$\frac{\delta \ell}{\varepsilon_u b^2} = \frac{P \ell}{\sigma_u t b^2} \left[\frac{1}{4} \left(\frac{\ell}{b} \right)^3 + \frac{3}{2} \left(\frac{\ell}{b} \right)^2 g \left(\frac{a}{b} \right) \right] \quad (11)$$

where $\varepsilon_u = \sigma_u/E$. The term comprised between the square brackets is a dimensionless compliance, which is a function of the relative crack depth, a/b , as well as of the beam slenderness, ℓ/b . Different load-deflection curves are represented in Figure 10 by varying the relative crack depth, a/b , and considering a constant ratio $\ell/b = 4$. On each linear plot in Figure 10, the point of ultimate strength and that of fracture propagation can be found using equations (6) and (8). In contrast to the latter, which is a single value, the former is dependent on the Brittleness Number s . A virtual load-deflection path is formed by the set of crack propagation points for which s is constant and by

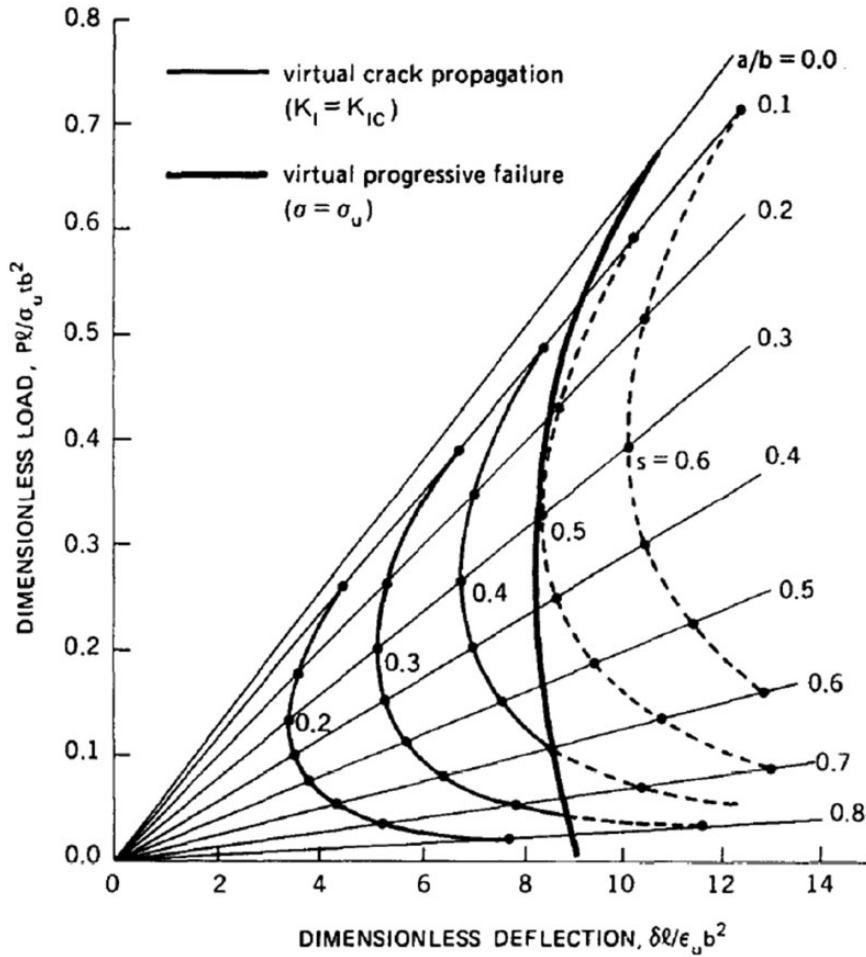


Figure 10. Nondimensional load of crack instability versus nondimensional deflection.

changing the relative crack depths. On this path, the considered load produces crack instability point by point.

When the crack grows, the instability load decreases and the compliance increases, so that the product on the right-hand side of equation (11) may prove to be either decreasing or increasing. The diagrams of Figure 10 show the deflection decreasing (with the load) up to the crack depth $a/b \sim 0.3$, and then increasing (in discordance with the load). Therefore, whereas for $a/b > 0.3$ the P - δ curve presents the usual softening path having a negative derivative, for $a/b < 0.3$ it presents a positive derivative. Such a branch could not be detected by deflection-controlled testing, and the representative point would jump from the positive to the negative branch with a discontinuity in the behaviour (snap-back instability).

The set of the ultimate strength points, for varying relative crack depths, is represented by the thick line in Figure 10. This line intersects the virtual crack propagation curves for $s \leq s_0 = 0.50$, which is analogous to what emerges from Figure 9.

In addition, the crack mouth opening displacement (CMOD), w_1 , is a function of the beam geometry and of the elastic modulus (Tada et al., 1973)

$$w_1 = \frac{6Pl a}{tb^2 E} p\left(\frac{a}{b}\right) \quad (12)$$

where $p\left(\frac{a}{b}\right)$ represents a suitable shape function.

In nondimensional form, equation (12) becomes

$$\frac{w_1 \ell}{\varepsilon_u b^2} = \frac{P \ell}{\sigma_u t b^2} \left[6 \left(\frac{\ell}{b}\right) \left(\frac{a}{b}\right) p\left(\frac{a}{b}\right) \right] \quad (13)$$

The term comprised between the square brackets represents the dimensionless compliance that, also in this case, depends on crack depth and beam slenderness. Figure 11 presents different load-CMOD curves by varying relative crack depths a/b and with constant ratio $\ell/b = 4$.

Also in this case, a virtual process is represented by the set of crack propagation points for constant s and varying relative crack depths. For all values of a/b , when the crack opens, the product on the right-hand side of equation (13) always increases, being the compliance increase overcoming the critical load decrease. The crack mouth opening displacement w_1 increases even when both deflection and load decrease in the catastrophic P - δ branch. Therefore, the P - w_1 curve presents always a negative derivative. If the process is controlled by the crack mouth opening displacement, i.e., if w_1 increases monotonically without discontinuities, the virtual P - δ path with positive slope could be followed regularly (without jumps or drops) (Carpinteri, 1989).

Progressive micro-cracking coalescence: Multiple snap-back instabilities

In the current section, an application of the crack length control scheme is presented in order to analyse the damage evolution in solids containing a distribution of collinear interacting micro-cracks in front of a macro-crack (Carpinteri and Accornero, 2018; Portela et al., 1993; Saleh and Aliabadi, 1995; Salgado and Aliabadi, 1996; Schlangen and van Mier, 1992; van Mier, 1991). During the incremental loading process, the macro-crack length is extended in order to achieve a slow and controlled propagation of the damage. Some examples are shown with regard to finite plates under plane strain conditions with one row of uniformly spaced collinear micro-cracks.

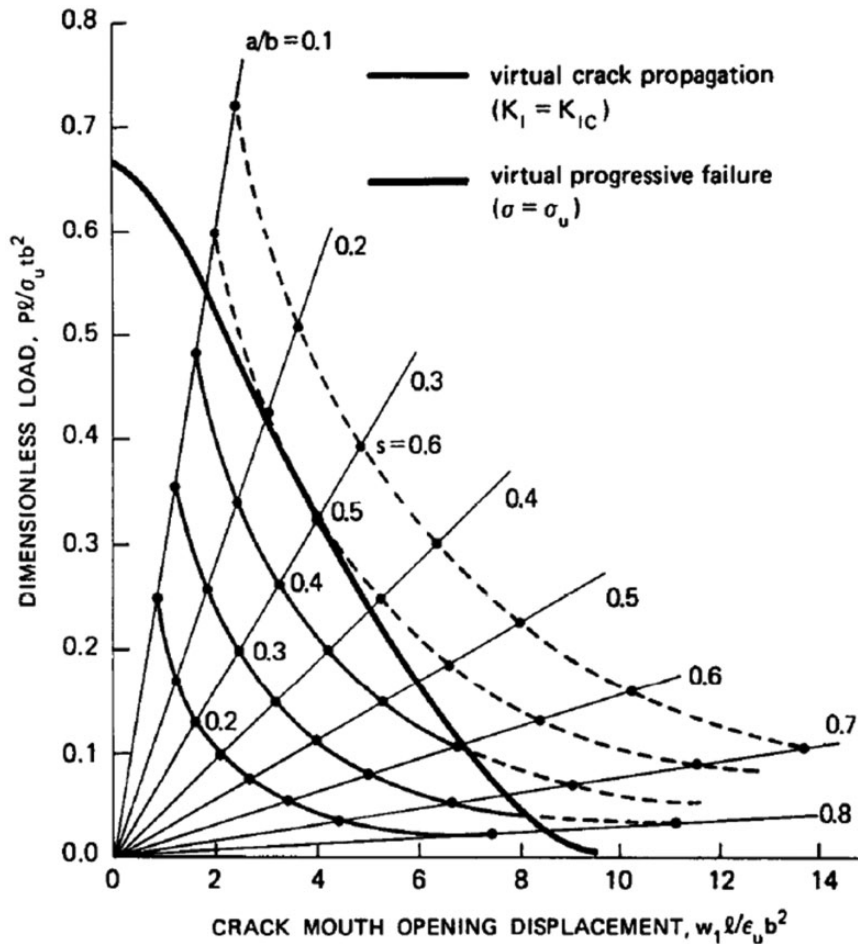


Figure 11. Nondimensional load of crack instability versus nondimensional crack mouth opening displacement.

Then, the effect of crack interaction on the evolution of damage is examined (Crouch and Starfield, 1983; Horii and Nemat-Nasser, 1985; Kachanov, 1985, 1993; Ortiz, 1988; Portela et al., 1992; Portela and Aliabadi, 1992; Portela and Santana, 2016) and multiple snap-back branches of the load-displacement curve are obtained numerically. Consider the case of a finite plate of width $2b$ with a central macro-crack of initial length $2a_0$ and with $2n$ initial collinear micro-cracks equally spaced between the corresponding tips. The plate is subjected to a uniaxial traction, σ , as shown in Figure 12. The loading process is controlled by the macro-crack length, which is always growing perpendicularly to the direction of traction.

The measure of the pre-existing damage, D , is defined as the ratio of the sum of the micro-crack initial lengths to the ligament ($D=0$ means absence of micro-cracks, i.e., undamaged ligament, whereas $D=1$ represents total separation). It is worth noting that the evolution of the propagation is also symmetric.

In Figures 13 to 16, some numerical tests considering the geometry of Figure 12 are reported in terms of stress-strain diagrams. The different curves are obtained by varying the initial damage

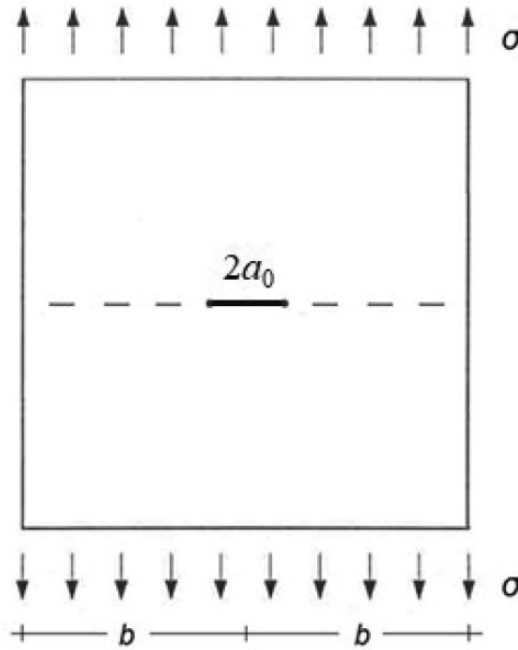


Figure 12. Finite plate subjected to uniaxial traction with a central dominant crack and a distribution of collinear micro-cracks.

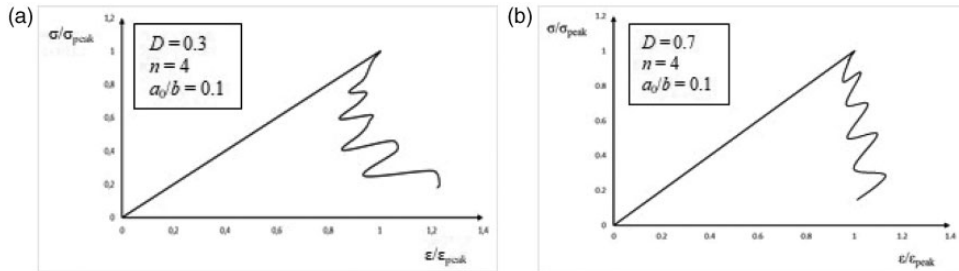


Figure 13. Normalized stress-strain diagrams of different micro-cracking coalescence case studies with $a_0/b = 0.1$. (a): $D = 0.3$; $n = 4$ and (b): $D = 0.7$; $n = 4$.

ratio, D , the number of collinear micro-cracks, n , and the initial relative length of the dominant crack, a_0/b . In this way, the snap-back instabilities in the global structural response are numerically captured, and the crack interaction effects are analyzed with respect to fracture evolution.

We can observe that, by increasing the initial damage ratio, D , the post-critical softening branch tends to decrease its slope. In Figures 13 and 14, the global snap-back phenomenon is less and less severe as D increases. As regards the influence of the number of micro-cracks, it can be observed that, by varying n , there is no substantial change in the global response, although it modifies the number and relevance of the single local snap-back. In addition, by comparing the four cases related to $a_0/b = 0.1$ (Figures 13 and 14), with those related to $a_0/b = 0.3$ (Figures 15 and 16), a transition

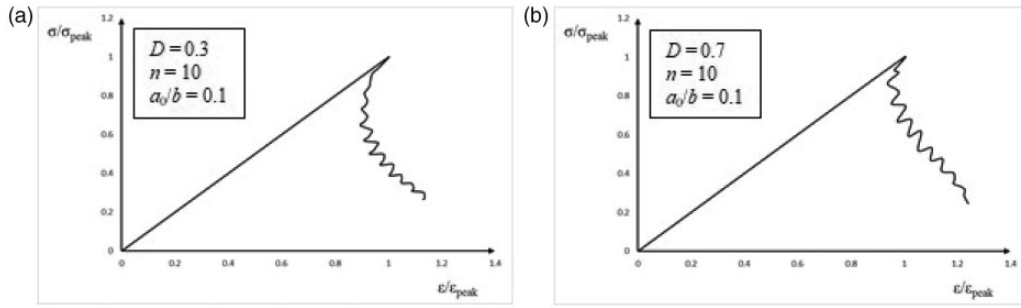


Figure 14. Normalized stress-strain diagrams of different micro-cracking coalescence case studies with $a_0/b = 0.1$. (a): $D = 0.3$; $n = 10$ and (b): $D = 0.7$; $n = 10$.

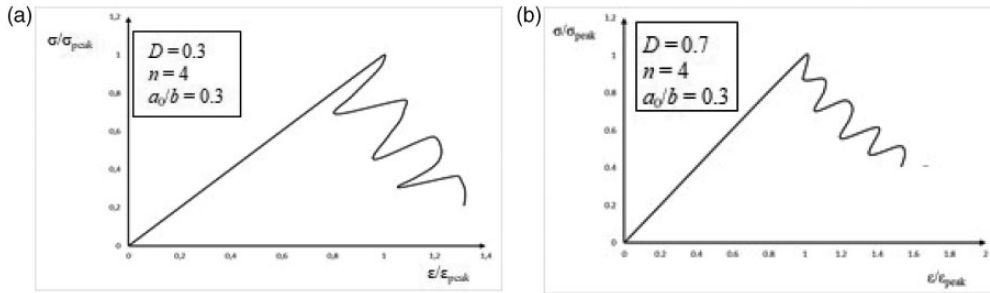


Figure 15. Normalized stress-strain diagrams of different micro-cracking coalescence case studies with $a_0/b = 0.3$. (a): $D = 0.3$; $n = 4$ and (b): $D = 0.7$; $n = 4$.

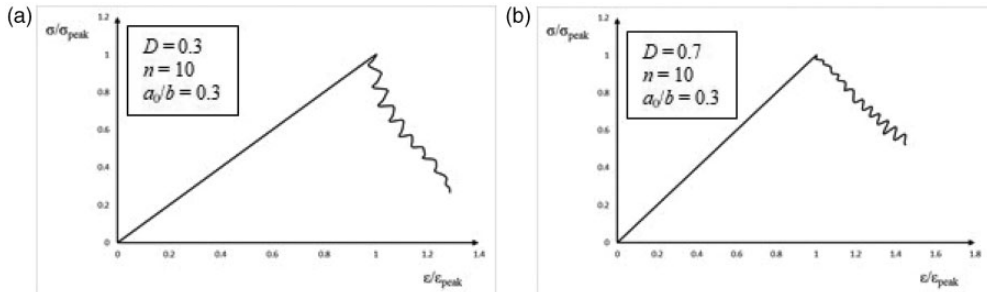


Figure 16. Normalized stress-strain diagrams of different micro-cracking coalescence case studies with $a_0/b = 0.3$. (a): $D = 0.3$; $n = 10$ and (b): $D = 0.7$; $n = 10$.

from a global snap-back instability to a global softening behaviour is evidenced. Therefore, by increasing the initial length of the dominant crack, a_0 , and keeping D and n unchanged, a decrease in the global brittleness of the specimen is detected.

In conclusion, a sharp global snap-back instability is identified in the case-studies with small initial damage ratios and/or short initial dominant cracks. On the contrary, a small and/or damaged ligament can avoid snap-back instabilities presenting a post-peak softening response.

Fibre-reinforced brittle-matrix composites: Multiple snap-back instabilities

The Updated Bridged Crack Model (UBCM) allows to investigate the post-cracking flexural behaviour of fibre-reinforced brittle-matrix structural elements, taking into account the elastic-perfectly brittle response of the matrix together with a cohesive softening law of the fibre-reinforcements (Accornero et al., 2022a, b, c; Carpinteri, 1981, 1984). Different versions of this model have been used to describe the fracture behaviour of fibre-reinforced composites as well as of materials reinforced by a rather small number of elements (Bosco and Carpinteri, 1992, 1995; Carpinteri and Massabò, 1997). In both cases, UBCM is able to explain and reproduce the constitutive flexural response that is often discontinuous owing to the presence of virtual catastrophic branches, i.e., snap-through and snap-back branches due to fibre action and matrix brittleness, respectively (Abdallah et al., 2018; Abdallah and Rees, 2019; Accornero et al., 2020, 2022a, 2022b; Banjara and Ramanjaneyulu, 2018; Bayramov et al., 2004; Boulekbatche et al., 2016; Campione et al., 2001; Carlesso et al., 2019; Carpinteri et al., 2023; Carpinteri and Accornero, 2019, 2020; Enfedaque et al., 2021; Fataar et al., 2021; Germano et al., 2016; Goel et al., 2012; Güvensoy et al., 2004; Hasegawa et al., 1989; Horii and Nemat-Nasser, 1985; Jun and Mechtcherine, 2010; Paschalis and Lampropoulos, 2016; Schäfer et al., 2021; Sornette et al., 1998). In addition, scale effects are considered as fundamental for a correct comprehension of the global structural behaviour, which can range from ductile to catastrophic simply by varying a dimensionless number, the Reinforcement Brittleness Number, N_P , which is a function of the matrix fracture toughness, K_{IC} , of the slippage strength of the fibre-reinforcement, $\bar{\sigma}_s$, of the fibre volume fraction, V_f , and of the characteristic structural size, b (Accornero et al., 2022; Carpinteri, 1981; 2021):

$$N_P = V_f \frac{\bar{\sigma}_s}{K_{IC}} b^{1/2} \quad (14)$$

In the following, the analyses performed by UBCM consider different fibre-reinforced brittle-matrix rectangular cross-section beams with slenderness equal to 4 and an initial notch of depth a_0 .

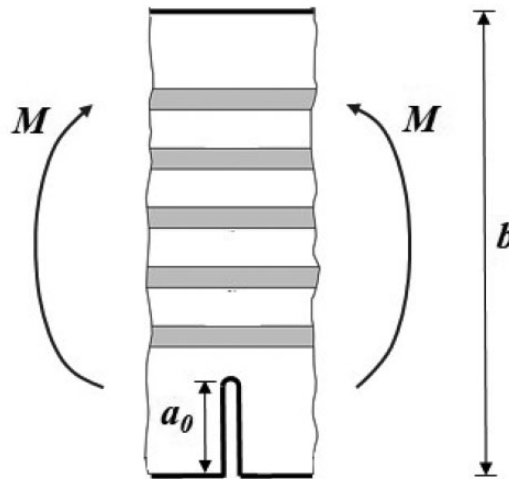


Figure 17. Fibre-reinforced brittle-matrix beam cross-section.

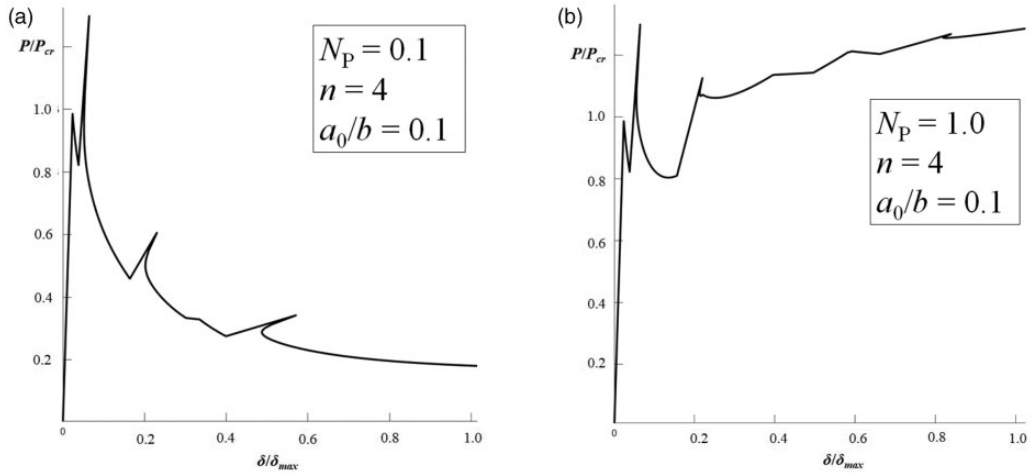


Figure 18. Normalized load-deflection diagrams of different fibre-reinforced brittle-matrix beams with $a_0/b = 0.1$. (a): $N_P = 0.1$; $n = 4$ and (b): $N_P = 1.0$; $n = 4$.

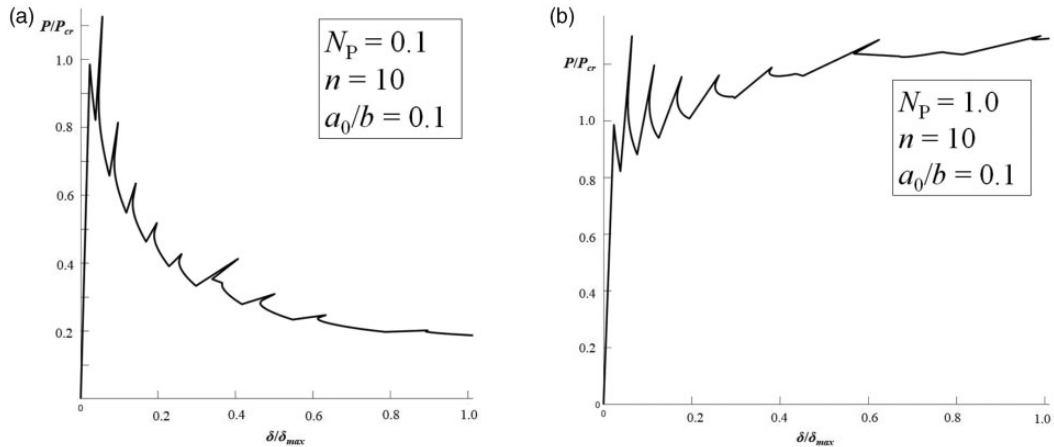


Figure 19. Normalized load-deflection diagrams of different fibre-reinforced brittle-matrix beams with $a_0/b = 0.1$. (a): $N_P = 0.1$; $n = 10$ and (b): $N_P = 1.0$; $n = 10$.

The scheme of the cracked beam section together with the position of the n parallel fibres ahead of the crack tip are shown in Figure 17.

In Figures 18 to 21, the normalized load-deflection diagrams of different numerical tests are reported, in which the geometry of Figure 17 is considered by varying the Reinforcement Brittleness Number, N_P , the number of parallel fibres, n , and the initial relative crack depth, a_0/b . In this way, the snap-back branches of the load vs. deflection curve are numerically captured, and the effects of the fibres interaction on fracture evolution are analyzed.

It is worth noting the crucial role played by the Reinforcement Brittleness Number, N_P : moving from lower to higher N_P values, the global post-cracking response changes from strain-softening to

strain-hardening. In this respect, a comparison can be made between the case of micro-cracking coalescence and that of fibre-reinforcements.

It can be observed that, by varying n , there is no change in the global response, although it modifies the number and relevance of the single local snap-back. As regards the influence of the notch depth, by comparing the cases related to $a_0/b=0.1$ (Figures 18 and 19), with those related to $a_0/b=0.3$ (Figures 20 and 21), and keeping N_P and n unchanged, an increase in the global ductility of the specimen is detected, i.e., the slope of the softening branch decreases (Figures 18(a), 19(a), 20(a) and 21(a)), whereas the slope of the hardening branch increases (Figures 18(b), 19(b), 20(b) and 21(b)).

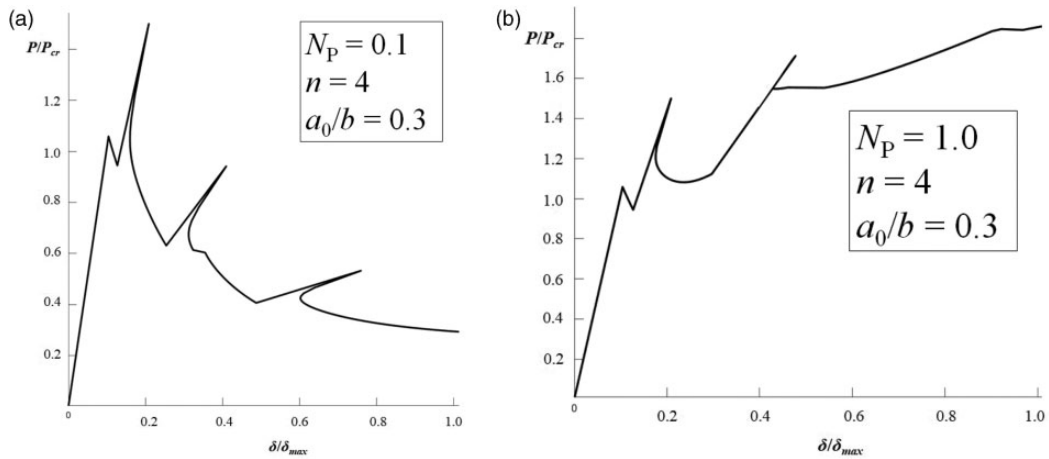


Figure 20. Normalized load-deflection diagrams of different fibre-reinforced brittle-matrix beams with $a_0/b = 0.3$. (a): $N_P = 0.1$; $n = 4$ and (b): $N_P = 1.0$; $n = 4$.

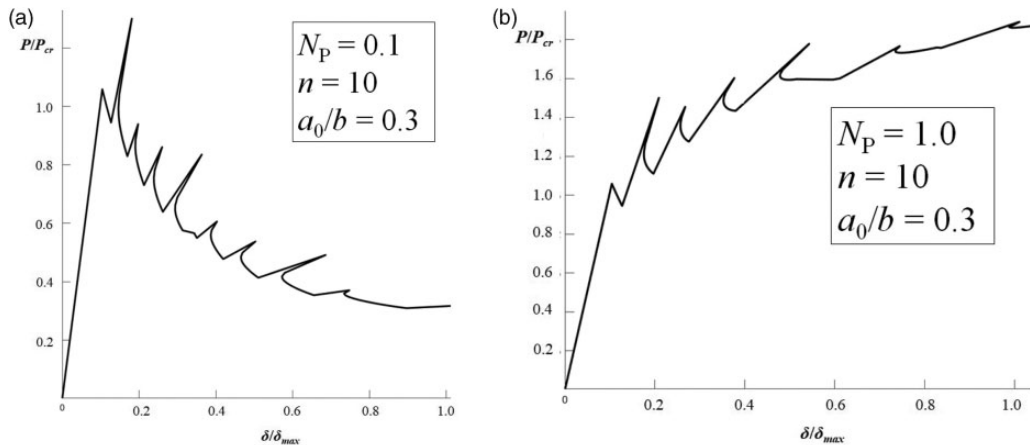


Figure 21. Normalized load-deflection diagrams of different fibre-reinforced brittle-matrix beams with $a_0/b = 0.3$. (a): $N_P = 0.1$; $n = 10$ and (b): $N_P = 1.0$; $n = 10$.

Conclusions

In the present work, the structural response of two brittle-matrix specimens is analysed: the first contains a distribution of collinear micro-cracks, whereas the second presents multiple parallel reinforcing fibres embedded in the matrix. In both cases, it is shown that the structural response presents a discrete number of snap-back instabilities with related peaks and valleys, the crack propagation occurring alternately within the matrix and through the heterogeneities. A strong analogy emerges between traversing weakened or strengthened zones, consisting in a multiple snap-back mechanical response, where descending branches of propagating cracks alternate with ascending branches of arrested cracks. In addition, the damage ratio, D , or the Reinforcement Brittleness Number, N_P , prove to govern the ductile-to-brittle transition occurring in the weakened specimen or in the strengthened one, respectively. Moving from lower to higher D or N_P values, the slope of the post-cracking branch changes from snap-back to strain-softening or from strain-softening to strain-hardening.


Declaration of conflicting interests

The author(s) declared no potential conflicts of interest with respect to the research, authorship, and/or publication of this article.

Funding

The author(s) disclosed receipt of the following financial support for the research, authorship, and/or publication of this article: This project has received funding from European Union's Horizon 2020 Research and Innovation Programme under Grant Agreement No. 951974. This work reflects only the authors' view and the Commission is not responsible for any use that may be made of the information it contains.

ORCID iD

Federico Accornero  <https://orcid.org/0000-0002-9638-8411>

References

- Abdallah S, Fan M and Rees DWA (2018) Bonding mechanisms and strength of steel fiber-reinforced cementitious composites: Overview. *Journal of Materials in Civil Engineering ASCE* 30(3): 04018001.
- Abdallah S and Rees DWA (2019) Analysis of pull-out behaviour of straight and hooked end steel fibres. *Engineering* 11(6): 332–341.
- Accornero F, Rubino A and Carpinteri A (2020) Ductile-to-brittle transition in fibre-reinforced concrete beams: Scale and fibre volume fraction effects. *Material Design & Processing Communication* 2(6): e127.
- Accornero F, Rubino A and Carpinteri A (2022a) Post-cracking regimes in the flexural behaviour of fibre-reinforced concrete beams. *International Journal of Solids and Structures* 248: 111637.
- Accornero F, Rubino A and Carpinteri A (2022b) Ultra-low cycle fatigue (ULCF) in fibre-reinforced concrete beams. *Theoretical and Applied Fracture Mechanics* 120: 103392.
- Accornero F, Rubino A and Carpinteri A (2022c) A fracture mechanics approach to the design of hybrid-reinforced concrete beams. *Engineering Fracture Mechanics* 275: 108821.
- Banjara NK and Ramanjaneyulu K (2018) Experimental investigations and numerical simulations on the flexural fatigue behavior of plain and fiber-reinforced concrete. *Journal of Materials in Civil Engineering ASCE* 30(8): 04018151.
- Barenblatt GI (1962) The mathematical theory of equilibrium cracks in brittle fracture. *Advances in Applied Mechanics* 7: 55–129.
- Bayramov F, Aydoner T, Ilki A, et al. (2004) An optimum design for steel fiber reinforced concretes under cyclic loading. In: *Proceedings of FraMCoS-5*, Vail.

- Bigaj AJ and Walraven JC (1993) Size effect on the rotational capacity of plastic hinges in reinforced concrete beams. *CEB Bulletin D'Information* 218: 7–24.
- Bosco C and Carpinteri A (1992) Softening and snap-through behaviour of reinforced elements. *Journal of Engineering Mechanics* 118(8): 1564–1577.
- Bosco C and Carpinteri A (1995) Discontinuous constitutive response of brittle matrix fibrous composites. *Journal of the Mechanics and Physics of Solids* 43(2): 261–274.
- Boulekbache B, Hamrat M, Chemrouk M, et al. (2016) Flexural behavior of steel fibre-reinforced concrete under cyclic loading. *Construction and Building Materials* 126: 253–262.
- Campione G, Miraglia N and Papia M (2001) Mechanical properties of steel fibre reinforced lightweight concrete with pumice stone or expanded clay aggregates. *Materials and Structures* 34(4): 201–210.
- Carlesso DM, de la Fuente A and Cavalaro SHP (2019) Fatigue of cracked high performance fiber reinforced concrete subjected to bending. *Construction and Building Materials* 220: 444–455.
- Carpinteri A (1980) A fracture mechanics model for reinforced concrete collapse. In: *Proceedings of the international conference on analytical and experimental fracture mechanics*, pp. 785–797. Sijthoff & Noordhoff, Alphen an den Rijn.
- Carpinteri A (1981) A fracture mechanics model for reinforced concrete collapse. In: *Proceedings of the IABSE colloquium on advanced mechanics of reinforced concrete*, Delft University Press, Delft, 17–30.
- Carpinteri A (1982) Notch sensitivity in fracture testing of aggregative materials. *Engineering Fracture Mechanics* 16(4): 467–481.
- Carpinteri A (1984) Interpretation of the Griffith instability as a bifurcation of the global equilibrium. In: *Proceedings of the NATO advanced research workshop on application of fracture mechanics to cementitious composites*, pp.287–316.
- Carpinteri A (1984) Stability of fracturing process in RC beams. *Journal of Structural Engineering* 110(3): 544–558.
- Carpinteri A (1989a) Cusp catastrophe interpretation of fracture instability. *Journal of the Mechanics and Physics of Solids* 37(5): 567–582.
- Carpinteri A (1989b) Post-peak and post-bifurcation analysis of cohesive crack propagation. *Engineering Fracture Mechanics* 32(2): 265–278.
- Carpinteri A (2021) *Fracture and Complexity: One Century since Griffith's Milestone*. Berlin: Springer.
- Carpinteri A and Accornero F (2018) Multiple snap-back instabilities in progressive microcracking coalescence. *Engineering Fracture Mechanics* 187: 272–281.
- Carpinteri A and Accornero F (2019) The bridged crack model with multiple fibres: Local instabilities, scale effects, plastic shake-down, and hysteresis. *Theoretical and Applied Fracture Mechanics* 104: 102351.
- Carpinteri A and Accornero F (2020) Residual crack opening in fibre-reinforced structural elements subjected to cyclic loading. *Strength, Fracture and Complexity* 12(2–4): 63–74.
- Carpinteri A and Accornero F (2021) Dimensional analysis of critical phenomena: Self-weight failure, turbulence, resonance, fracture. *Physical Mesomechanics* 24(4): 459–463.
- Carpinteri A and Massabò R (1997) Continuous vs discontinuous bridged crack model of fibre-reinforced materials in flexure. *International Journal of Solids and Structures* 34: 2312–2338.
- Carpinteri A, Accornero F and Rubino A (2023) Scale effects in the post-cracking behaviour of fibre-reinforced concrete beams. *International Journal of Fracture* 240(1): 1–16.
- Crouch SL and Starfield AM (1983) *Boundary Element Methods in Solid Mechanics with Applications in Rock Mechanics and Geological Engineering*. London: Allen and Unwin.
- Enfedaque A, Alberti MG, Gálvez JC, et al. (2021) Assessment of the post-cracking fatigue behavior of steel and polyolefin fiber-reinforced concrete. *Materials* 14(22): 7087.
- Fataar H, Combrinck M and Boshoff WP (2021) An experimental study on the fatigue failure of steel fibre reinforced concrete at a single fibre level. *Construction and Building Materials* 299: 123869.
- Germano F, Tiberti G and Plizzari G (2016) Post-peak fatigue performance of steel fiber reinforced concrete under flexure. *Materials and Structures* 49(10): 4229–4245.
- Goel S, Singh SP and Singh P (2012) Fatigue analysis of plain and fiber-reinforced self-consolidating concrete. *ACI Materials Journal* 109(5): 573–582.

- Goldstein RV and Vainshelbaum VM (1978) Material scale length as a measure of fracture toughness in fracture mechanics of plastic materials. *International Journal of Fracture* 14(2): 185–201.
- Gordon JE (1975) *The New Science of Strong Materials*. Princeton: Princeton University Press.
- Güvensoy G, Bayramov F, Ilki A, et al. (2004) Mechanical behavior of high performance steel fiber reinforced cementitious composites under cyclic loading condition. In: *Proceedings of the international symposium on ultra high performance concrete*, Kassel.
- Hasegawa A, Horii H and Nishino F (1989) Fracture process and bridging zone model and influencing factors in fracture of concrete. In: *Proceedings of the SEM-RILEM international conference on fracture of concrete and rock*, pp.205–219.
- Horii H and Nemat-Nasser S (1985) Elastic field of interacting inhomogeneities. *International Journal of Solids and Structures* 21(7): 731–745.
- Jun P and Mechtcherine V (2010) Behaviour of strain-hardening cement-based composites (SHCC) under monotonic and cyclic tensile loading: Part 1 – Experimental investigations. *Cement and Concrete Composites* 32(10): 801–809.
- Kachanov LM (1985) A simple technique of stress analysis in elastic solids with many cracks. *International Journal of Fracture* 28(1): R11–R19.
- Kachanov LM (1993) Elastic solids with many cracks and related problems. *Advances in Applied Mechanics* 30: 259–445.
- Kani GN (1967) How safe are our large concrete beams? *ACI Journal* 64: 128–141.
- Ortiz M (1988) Microcrack coalescence and macroscopic crack growth initiation in brittle solids. *International Journal of Solids and Structures* 24(3): 231–250.
- Paschalis SA and Lampropoulos P (2016) Ultra-high-performance fiber-reinforced concrete under cyclic loading. *ACI Materials Journal* 113(4): 419–427.
- Portela A and Aliabadi MH (1992) *Crack Growth Analysis using Boundary Elements*. Southampton, UK: Computational Mechanics Publications.
- Portela A and Santana E (2016) Dual boundary element analysis of fatigue crack growth, interaction and linkup. *Engineering Analysis with Boundary Elements* 64: 176–195.
- Portela A, Aliabadi MH and Rooke DP (1992) The dual boundary element method: Effective implementation for crack problems. *International Journal for Numerical Methods in Engineering* 33(6): 1269–1287.
- Portela A, Aliabadi MH and Rooke DP (1993) Dual boundary element incremental analysis of crack propagation. *Computers & Structures* 46(2): 237–247.
- Rots JG and de Borst R (1987) Analysis of mixed-mode fracture in concrete. *Journal of Engineering Mechanics* 113: 1739–1758; discussion on the same paper by Carpinteri A and Valente S (1989). *Journal of Engineering Mechanics* 115: 2344–2347.
- Saleh AL and Aliabadi MH (1995) Crack growth analysis in concrete using boundary element method. *Engineering Fracture Mechanics* 51(4): 533–545.
- Salgado NK and Aliabadi MH (1996) The application of the dual boundary element method to the analysis of cracked stiffened panels. *Engineering Fracture Mechanics* 54(1): 91–105.
- Schäfer N, Gudzulic V, Breitenbücher R, et al. (2021) Experimental and numerical investigation on high performance SFRC: Cyclic tensile loading and fatigue. *Materials* 14(24): 7593.
- Schlangen E and van Mier JGM (1992) Experimental and numerical analysis of micromechanisms of fracture of cement-based composites. *Cement and Concrete Composites* 14(2): 105–118.
- Sornette D, Leung KT and Andersen JV (1998) Conditions for abrupt failure in the democratic fiber bundle model. *Physical Review Letters* 80: 3158.
- Tada H, Paris PC and Irwin GR (1973) *The Stress Analysis of Cracks Handbook*. Bethlehem, Pennsylvania: Del. Research Corporation.
- Tanabe T, Itoh A and Ueda N (2004) Snapback failure analysis for large scale concrete structures and its application to shear capacity study of columns. *Journal of Advanced Concrete Technology* 2(3): 275–288.
- Tang T, Shah SP and Ouyang C (1992) Fracture mechanics and size effect of concrete in tension. *Journal of Structural Engineering* 118(11): 3169–3185.

- Tassava CJ (2003) Weak seams: Controversy over welding theory and practice in American shipyards 1938–1946. *History and Technology* 19(2): 87–108.
- Thomason JL and Vlug MA (1996) Influence of fibre length and concentration on the properties of glass fibre-reinforced polypropylene: Tensile and flexural modulus. *Composites Part A: Applied Science and Manufacturing* 27(6): 477–484.
- Tipper C (1962) *The Brittle Fracture Story*. Cambridge: Cambridge University Press.
- van Mier JGM (1991) Mode I fracture of concrete: Discontinuous crack growth and crack interface grain bridging. *Cement and Concrete Research* 21(1): 1–15.
- von Kármán T and Tsien HS (1941) The buckling of thin cylindrical shells under axial compression. *Journal of the Aeronautical Sciences* 8(8): 303–312.